Journal of Advanced Research in Applied Sciences and Engineering Technology

Journal homepage:
https://semarakilmu.com.my/journals/index.php/applied_sciences_eng_tech/index
ISSN: 2462-1943

Impact Strain Signal Characteristics of Al and Mg under Instrumented Charpy Test

Hikmah Zainuddin[1], Mohd Basri Ali[2,*], Nurlaela Muhammad Said[1], Kamarul Ariffin Zakaria[1], Sivakumar Dhar Malingam[1], Mohd Hadzley Abu Bakar[2], Nor Fauzi Tamin[3]

[1] Faculty of Mechanical Technology and Engineering, Universiti Teknikal Malaysia Melaka, Hang Tuah Jaya, 76100 Durian Tunggal, Melaka, Malaysia
[2] Faculty of Industrial and Manufacturing Technology and Engineering, Universiti Teknikal Malaysia Melaka, Hang Tuah Jaya, 76100 Durian Tunggal, Melaka, Malaysia
[3] Faculty of Technical and Vocational Education, Universiti Tun Hussein Onn Malaysia, 86400 Batu Pahat, Johor, Malaysia

ARTICLE INFO

Article history:
Received 18 August 2023
Received in revised form 8 November 2023
Accepted 21 February 2024
Available online 2 April 2024

Keywords:

Charpy impact; Energy absorption; PSD energy; Impact duration; Impact strain signal

ABSTRACT

Impact strain signal is used to examine strain signal patterns under various parameters. Impact is a complicated phenomenon that occurs within a millisecond timeframe. Material toughness is measured by the energy absorption recorded by the Charpy machine and closely related to the specimen fracture deformation. By utilizing the strain gauge and data acquisition, the impact strain signal provides additional data regarding impact duration, maximum strain value and the area under curve for a deeper understanding of the impact problem. A material with high toughness has great energy absorption and the capability to withstand high impact load. Although magnesium is lighter in weight compared to aluminium, aluminium is a better corrosion-resistant material and is stronger, which makes it more suitable to be fabricated as automotive structural components. Tensile test is typically used for investigating a material's mechanical properties. In the automotive industry, materials are required to have good crashworthiness. This study investigates the relationship between the energy absorbed with the power spectral density and the area under strain–time graph for different materials, impact speeds, and material thicknesses. Furthermore, the relationship between the stress–strain curve and impact strain signal were examined. In this study, the behaviour of two materials, namely Aluminium 6061-T6 and Magnesium AM60, was investigated using instrumented Charpy test, by referring to the impact strain signal pattern result. For the experiment, strain gauge attached to the Charpy machine striker was employed and linked to the data acquisition system. Charpy impact specimen has three different thicknesses; 10 mm, 7.5 mm and 5 mm. Impact speed is at 3.35 m/s and 5.18 m/s. Results show a correlation between energy absorbed with strain energy. Strain energy obtained is directly proportional to the energy absorbed. Aluminium 6061-T6 has the highest energy absorption, maximum strain, and strain energy under power spectral density graph compared to Magnesium AM60. Relation of strain signal from Charpy test and stress–strain curve from tensile test shows a significant finding where the material deforms and fracture points are identified through the signal pattern and curve. Thus, the strain signal pattern can be used to predict material behaviour.

* *Corresponding author.*
E-mail address: basri@utem.edu.my

https://doi.org/10.37934/araset.42.2.1326

1. Introduction

Manufacturers in the automotive industry strive to serve the best quality to the consumer, especially with respect to the overall vehicle performance and safety. Main segments of an automobiles are the chassis and body, the engine and transmission system, as well as the interior part. In both moving and stationary states, each part shares and experiences various types of loading. Wheel is one of the crucial components of the vehicle transmission system, and alloy materials find extensive applications in wheel manufacturing because of their durability, lightweight, and balance with stylish aesthetic value. To ensure no negligence in the safety requirements, rotating bending test, radial fatigue test, and impact test are compulsory for wheel designing and producing prior to the mass production [1]. The safety performance evaluation primarily relies on two factors: the maximum impact force and the maximum energy absorption capacity [2]. The designed energy absorbing structure must be capable to absorb energy under dynamic impact or blast [3-5]. Impact testing is concerned with the evaluation of the material toughness under sudden force, which is determined by the value of energy absorbed. An excellent structure of energy absorber must be capable of dissipating the impact energy irreversibly through plastic deformation. Energy-absorbing structures have in some instances been made up of metallic thin-walled components because of their ability to deform plastically in the elastic–plastic behaviour [6-9]. Energy absorption during an impact test is influenced by a number of factors such as the impact condition, thickness, rib, material, and shape [11,12] Impact response of expanded metal tubes was performed by Graciano *et al.,* [13] and Borges *et al.,* [14], where the outcomes of the investigations revealed that the energy absorption response is influenced by expended tube size and cell orientation, as well as the impact velocity. Another study on instrumented Charpy impact employed a signal acquisition architecture, where the researchers compared the toughness measured by the Charpy machine dial gauge with the toughness calculated from the estimated load–displacement curve [15]. Strain gauges were also employed by previous researchers for the wheel impact test by attaching the strain gauges to the wheel disc [16,17]. Ali *et al.,* [18] analysed the correlation of impact energy with strain energy, and their results show that the energy absorbed capability, strain energy, and the power spectral density (PSD) peak are affected by the type of material, specimen thickness, and the impact speed. Furthermore, the higher value of energy absorbed produces a greater PSD peak as well as greater strain energy. Murali *et al.,* [19] performed the drop weight impact test on fibre-reinforced concrete to investigate the relationship between the impact energy and the compressive strength. Regression analysis was made and they developed an accurate and reliable empirical relationship to estimate the impact energy for the fibre-reinforced concrete. For a thin-walled structure experimented under quasi-static and dynamic axial loading, it was shown that the energy absorption capacity increase with the yield strength, wall thickness, and impact velocity [20]. Stiffer impact surface generally decreases the energy absorbed [21].

Along the lines of the above-mentioned studies, fewer studies have been conducted to correlate the energy absorbed with the strain energy attained from the impact strain signal. Nevertheless, these correlations are important in gaining deeper understanding of the complicated impact phenomenon, not only relying on the energy absorption value and fracture deformation. This study was conducted with the objective to attain the characterisation and classification of strain signal from the instrumented Charpy test and validated its effectiveness as an alternative method to predict the material properties. To investigate the relationship between the impact strain signal with the stress–strain curve, tensile test was conducted, which yielded this curve. The instrumented Charpy impact test data were used to get the energy absorption, impact strain signal, maximum strain behaviour, and impact duration. Lastly, the effect of material thickness was also studied.

2. Literature Review

The most commonly employed impact tests for determining a material's energy-absorbing ability are the Charpy test, Izod test, and drop test. Among these, Charpy test is the most popular choice because of its reliability and ease in conduction with low cost of execution. In the Charpy impact test, the impact energy absorbed recorded represents the energy required to fracture the test specimen. This method is as well an economical quality control method to determine impact material toughness and the notch sensitivity, where the notched area is a stress concentrated region and certain materials are more sensitive to notches compared to other [22]. The energy absorption performance can be calculated from the integration of the load–displacement curve, expressed by Eq. (1) [5].

$$EA = \int_0^{\delta b} P.d\delta = P_m(\delta b - \delta l) \quad (1)$$

P_m = mean crushing load
δb = length of the crushing specimen
δl = initial length of the crushing specimen

In extent to the Charpy impact test, researchers had performed an instrumented Charpy impact test where strain gauges were connected to the impact striker to capture the dynamic impact strain response [1,18,23]. The recorded signal in the time domain was converted to the frequency domain that is presented in Power Spectral Density (PSD). The area under the PSD curve was used to calculate strain energy. There are good correlation between the energy absorbed and the strain energy [1,18]. These results match with the earlier study made by Shterenlikht *et al.,* [23]. They found that the strain energy calculated agrees well with the energy collected from the machine. All this correlation notes that PSD is a reliable alternative method for the Charpy impact test data measurement.

Even though the tensile test and impact test are dissimilar due to their different parameters to define a material strength, somewhat researchers show great interest in relating the two methods to save time and cost. Driven by the idea of discovering another way to acquire mechanical properties that are usually obtained by using the tensile test, Alar *et al.,* [24] executed the instrumented Charpy impact test that allowed them to gather the result in term of the force-displacement curve and later compared the result with the tensile test. The yield force and maximum force from both tests indicated a good correlation between each other. Further study by Alar & Mandić [25] has explored other mechanical properties from the instrumented Charpy impact, which is the yield strength and tensile strength. Comparing them with the tensile test outcome, the percentage of differences were found to be 4% and 5% only.

Another approach to determining the mechanical properties of material was discovered by Ramli *et al.,* [26]. During the steel ball impact test, the vibration signal produced by the ball was captured by using 4 accelerometer sensors placed on the specimens. The work is initiated to develop an alternative method based on signal analysis using accelerometer sensors known as I-Kaz 4 channels to characterize several mechanical properties such as Poisson Ratio, Vickers Hardness, Yield Strength, Tensile Strength, Compression Strength, and Fatigue Strength. There is a correlation between the I-Kaz linear coefficient and material mechanical properties, with an R square value of 0.969 to 0.997.

In this study, material selection was based on the commonly used material in the automotive industry, especially on components involving in the impact application. The aluminium alloy and magnesium alloy are some of the common materials used due to their lightweight characteristic, together with the exceptional energy absorption capacity. Magnesium alloy has high specific strength

with high specific energy, and is able to resist high deformation and tolerate high loads [27]. Magnesium AM60 has been used to fabricated as the casting part [28], chassis component [29] and wheel [30]. Meanwhile, aluminium is a popular material for many automotive applications since it is corrosion resistant and has a good formability [31], with high strength to weight ratio [32]. Some of the common automotive parts made of Aluminium 6061-T6 are wheel [33] and vehicle crash box [34].

There are several work emphases on the correlation between the tensile test and impact test. Previously, researchers used strain signal to captured the vibration signal. It is possible that the instrumented Charpy impact able to predict the material behaviour instead of executing tensile test as the primary method to obtain the mechanical properties. On that note, it gives an idea to explore the research gap in this field to develop an alternative method to predict the material behaviour by utilizing the impact strain signal, its characteristics and patterns.

3. Methodology

3.1 Material Preparation

In addition to being lightweight and having great strength, a wheel should have good durability and resistance to corrosion. Alloy materials are widely used in automotive wheels, and because of this, Aluminium 6061-T6 and Magnesium AM60 were selected in this study. The material properties of the materials are summarised in Table 1. Carbon Steel 1050 material properties are presented as well. Magnesium AM60 is brittle and has low value of Young's modulus, whereas Aluminium 6061-T6 is ductile and has a high value of Young's modulus.

Table 1
Material Properties

Material properties	Aluminium 6061-T6	Magnesium AM60	Carbon Steel 1050 [35]
Young's modulus (GPa)	67.60	6.60	200
Poisson's ratio	0.30	0.35	0.30
Density (kg/m3)	2700	1800	7860

Charpy impact test specimen was designed in accordance with the American Standard for Testing and Material (ASTM) E23. It has length, height, and width of 55 mm, 10 mm, 10 mm, respectively. The specimen type is the v-notch type, v-notch of 45º with root radius 0.25 mm and depth 2 mm. Specimens with thicknesses 5 mm and 7.5 mm were also prepared. In each parametric study, five specimens were prepared. Meanwhile, the tensile test specimen was designed in dog-bone shape by referring to the ASTM E8 and three samples were tested for each material.

3.2 Experimental Work

The Charpy impact test was conducted following the ASTM E23 and executed at room temperature of 23ºC ± 5ºC. The experimental setup in this study is similar as previous researchers [18]. Two different impact speeds were set and the speed was determined by the latch position: 3.35 m/s at low latch position and 5.18 m/s at high latch position. Figure 1 shows the apparatus and instrument used in the experimental work: The Charpy machine, model SI-1C3 with capacity of 406.7 J, strain gauge, data acquisition system (SOMAT eDAQ), and a computer.

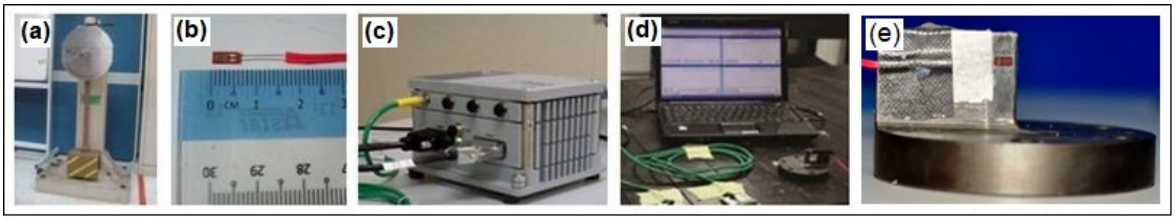

Fig. 1. Apparatus and instrument used in Charpy test: (a) Charpy machine 406 J, (b) Strain gauge, (c) Data acquisition system (eDAQ), (d) Computer as result display, (e) Strain gauge glued on the impactor

The tensile test was carried out using the universal testing machine (UTM) model Instron 8872 with capacity of 25 kN. The test was performed in accordance with ASTM E8, at room temperature with crosshead speed of 2 mm/min. The data were displayed as the stress–strain curve in order to extract the material properties such as the Young's modulus, Poisson's ratio, yield strength, and ultimate strength. the stages and formulas that are used in data analysis, arranged sequentially step by step

3.3 Data Analysis

The tensile test provides important mechanical properties such as the ultimate tensile strength, yield strength, Young's modulus and Poisson's ratio. These properties were extracted from the stress-strain curve plotted upon the completion of tensile test. Aside, the deformation of the specimen was observed for better understanding of necking point and fracture point during the experiment.

Energy absorbed from the Charpy test was directly measured by the scale of the machine. Relatively, for strain signal analysis, the strain signal was analysed in the time domain and frequency domain. The frequency domain was presented in the PSD. Initially, results of impact strain signal in 'SIE' format were imported into InField software for result optimisation. During the Charpy test, the impact took place in millisecond, and the strain signal deformation captured was too small. Hence, the data were optimised and enlarged to the particular deformed area, limiting to a duration of 0 to 3.5 milliseconds. For further analysis, strain–time graphs and power spectral density were plotted to identify the strain signal parameters, namely the maximum strain, impact duration, and area under graph.

Subsequently, the analysis includes the relation of strain signal patter with the stress-strain curve. For the purpose of finding the relation between impact test and tensile test, the impact strain signal pattern was correlated with the stress–strain curve. The graph pattern was then compared at the deformation and fracture point of the specimen. The chosen impact strain signal was the 10 mm thickness at 5.18 m/s result, and it was compared with the tensile test stress–strain graph for the Aluminium 6061-T6 and Magnesium AM60, as well as Carbon Steel 1050.

In the final analysis, the impact strain signal was characterised and classified according to the results of the Charpy test strain signal pattern, at 10 mm thickness with impact speed 5.18 m/s. The speed of 5.18 m/s was chosen because high speed in crash event gives more significant effect compared to a speed of 3.35 m/s. The strain signal characteristics and classification were identified based on the energy absorbed, maximum strain, impact duration, area under the graph, and the shape of the signal plotted.

4. Results and Discussion

4.1 Energy Absorption Behaviour

Different parameters exhibited different energy absorbing ability. The average energies absorbed for the impact test for both materials are recorded in Table 2. At a low speed, 3.35 m/s with specimen thickness of 10 mm, both materials experienced high impact energy absorbed, while at a high speed and minimum thickness of 5 mm, the energy absorbed capacity was found to be low. Thin material impacted under high velocity was easily damaged and fractured compared to thick material with lower impact velocity [36]. This reveals that the energy absorption performance is influenced by the specimen thickness and the impact speed, as demonstrated in Figure 2(a). Graph pattern in Figure 2(a) shows that the energy absorbed has a positive relationship with the specimen thickness but acts inversely towards the impact speed. Decrease in Charpy specimen thickness reduces the area under the notch and consequently the notch toughness [37]. Meanwhile, thicker composite layer produces thicker specimen and thus increases the impact energy [38]. Previous researchers had noticed that the increment in impact speed leads to a decrement in energy absorption capacity [13]. Besides, higher impact speed caused early failures in the impacting event [39].

Table 2
Average energy absorbed of Aluminium 6061-T6 and Magnesium AM 60 at different parameters

Thickness (mm)	Average absorbed energy (J) for Aluminium 6061-T6		Average absorbed energy (J) for Magnesium AM60	
	Speed at 3.35 m/s	Speed at 5.18 m/s	Speed at 3.35 m/s	Speed at 5.18 m/s
5.0	15.40 ± 1.34	10.00 ± 2.00	6.00 ± 0.71	1.60 ± 0.55
7.5	20.20 ± 0.45	13.20 ± 1.10	8.20 ± 0.84	2.80 ± 0.84
10.0	24.80 ± 2.59	20.40 ± 1.67	9.20 ± 0.84	3.60 ± 0.55

Impact strain is the deformation of the specimen due to the impact loading. Maximum strain (ε_{max}) is the highest peak of strain in the strain–time graph. For each material and condition of variable thickness and impact speed, the average maximum strain was calculated (see Table 3). The negative strain value implies that the specimen experienced compression during the Charpy test.

Table 3
Average maximum strain of Aluminium 6061-T6 and Magnesium AM60 at different parameters

Thickness (mm)	Average maximum strain, εmax (με) (Aluminium)		Average maximum strain, εmax (με) (Magnesium)	
	Speed at 3.35 m/s	Speed at 5.18 m/s	Speed at 3.35 m/s	Speed at 5.18 m/s
5.0	−103.62 ± 4.54	−104.50 ± 8.59	−42.36 ± 1.52	−45.94 ± 2.00
7.5	−164.96 ± 11.43	−167.92 ± 20.47	−56.20 ± 2.41	−57.82 ± 0.97
10.0	−196.91 ± 6.51	−199.86 ± 16.03	−59.01 ± 8.69	−60.02 ± 4.76

According to the data in Table 3, thicker specimen with high-speed impact has the greatest value of maximum strain, which is −199.86 με and −60.02 με for Aluminium 6061-T6 and Magnesium AM60, respectively. Hence, low impact speed has the lowest maximum strain value, which is −103.62 με and −42.36 με for Aluminium 6061-T6 and Magnesium AM60, respectively. Regardless of the speed applied, 10 mm thickness contained the highest strain amplitude compared to 5 mm thickness for both materials. Authors of a previous study have reported that the maximum displacement value increases with the increase in impact velocity [39]. As the value of strain increase following the material deformation, maximum deformation leads material to have maximum strain. The deformation is associated with the strength of the bonds between atoms in the solid structure [49].

Lattice structure of aluminium is in form of face-centred cubic (fcc), whereas magnesium is in hexagonal close-packed (hcp) form, which explains their fundamental differences in forming behaviour [40]. Metal with fcc has better plastic deformation together with its ductile behaviour compared to hcp lattice metal [42]. Ivañez *et al.,* [43] concluded that the increase in impact speed gives out greater value of maximum displacement. The effect of specimen thickness and impact speed on the maximum strain value for different types of material is illustrated in Figure 2(b).

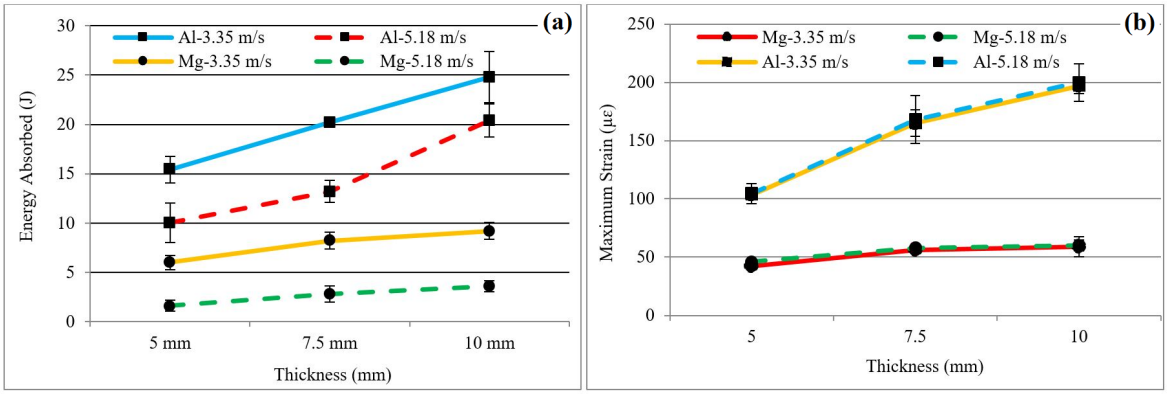

Fig. 2. (a) Energy absorbed at different sample thickness, (b) Maximum strain at different sample thickness

Points connected on the graph in Figure 2(b) shows that for the respective impact tests indicate that the maximum strain value increases with the increase in impact speed and material thickness. Referring to data in Table 3, for both materials, it appears that there is a slight increment on the maximum strain, which is around 1 με to 3 με when speed increases from 3.35 m/s to 5.18 m/s. It is worth noting that the increase in the impact speed in Charpy test does not give a significant effect on the maximum strain behaviour. Nevertheless, the increment in specimen thickness has caused the value of maximum strain to increase greatly for Aluminium 6061-T6, which is 61 με to 95 με, whereas Magnesium AM60 is still showing small increment, which is only 12 με to 17 με, due to its brittleness.

During a collision, longer impact duration is crucial to provide a considerable extended crush space for plastic deformation, especially in the automotive industry, which comprises occupant safety and protection. The average value of impact duration is shown in Table 4. For both materials, thicker specimen, which is subjected to low impact speed, exposed the highest impact duration at 2.01 ms and 1.12 ms for Aluminium 6061-T6 and Magnesium AM60, respectively.

Table 4
Average impact duration of Aluminium 6061-T6 and Magnesium AM60 at different parameters

Thickness (mm)	Average impact duration (ms) for Aluminium 6061-T6		Average impact duration (ms) for Magnesium AM60	
	Speed at 3.35 m/s	Speed at 5.18 m/s	Speed at 3.35 m/s	Speed at 5.18 m/s
5.0	1.50 ± 0.10	1.08 ± 0.07	0.92 ± 0.07	0.62 ± 0.05
7.5	1.78 ± 0.05	1.45 ± 0.12	1.02 ± 0.04	0.76 ± 0.05
10.0	2.01 ± 0.06	1.74 ± 0.06	1.12 ± 0.03	0.86 ± 0.08

Likewise, energy absorbed trends, the impact duration increases with material thickness, yet it decreases as the impact speed increases. Logically, thin material needed shorter duration and is easy to break. High impact speed produced high peak force and required less time to break a test piece and therefore lowers the impact duration.

4.2 Area Under Strain-Time Graph and PSD Graph

The area under strain–time graph represents the strain energy of a material while a PSD indicates the power content of strain signal per unit frequency. Table 5 and Table 6 show the average area under the strain-time graph and PSD graph respectively.

Table 5
Average area under ε–t graph of Aluminium 6061-T6 and Magnesium AM60 at different parameters

Thickness (mm)	Average area under ε–t graph (με.ms) for Aluminium 6061-T6		Average area under ε–t graph (με.ms) for Magnesium AM60	
	Speed at 3.35 m/s	Speed at 5.18 m/s	Speed at 3.35 m/s	Speed at 5.18 m/s
5.0	81.17 ± 5.22	56.14 ± 4.37	21.34 ± 2.88	12.70 ± 1.69
7.5	149.88 ± 10.92	105.77 ± 10.70	29.20 ± 3.90	19.36 ± 1.43
10.0	165.05 ± 27.00	133.01 ± 14.77	31.72 ± 4.14	25.46 ± 4.04

Table 6
Average area under PSD graph of Aluminium 6061-T6 and Magnesium AM60 at different parameters

Thickness (mm)	Average area under PSD (με2/Hz) for Aluminium 6061-T6		Average area under PSD (με2/Hz) for Magnesium AM60	
	Speed at 3.35 m/s	Speed at 5.18 m/s	Speed at 3.35 m/s	Speed at 5.18 m/s
5.0	1854.52 ± 80.67	1314.88 ± 203.53	239.07 ± 33.82	173.44 ± 39.78
7.5	5711.33 ± 638.07	3649.17 ± 899.67	379.28 ± 72.75	259.54 ± 16.93
10.0	7292.59 ± 1346.77	5840.61 ± 680.71	427.73 ± 108.89	383.03 ± 100.05

Significantly, the thickest material tested with speed of 3.35 m/s has the largest area under graph, Figure 3 illustrates the effect of thickness and speed for both graphs.

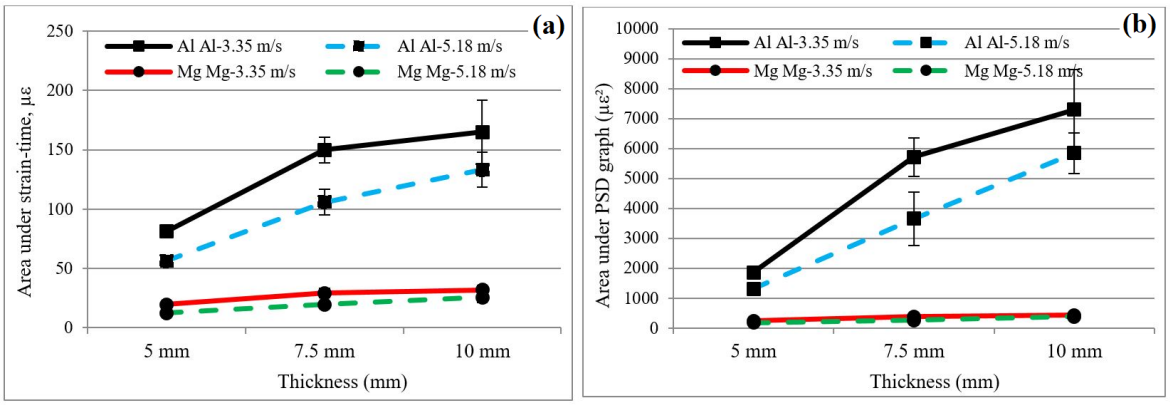

Fig. 3. Effect of thickness and speed (a) area under strain-time graph, (b) PSD graph

Based on Figure 3, the area under graph elevates when the material gets thicker, but the values go down as the speeding rate increases. As thick material has a high impact duration, the shape of strain signal is extended along the x-axis causing the area of signal pattern to become larger. A previous study on impact signal pattern supported that the material with lower thickness is easily damaged and fractured compared to those with greater thickness [44]. This clarifies that high speeding rate leads to shorter impact time and thus results in a smaller shape of strain signal. In both speed conditions–low and high—the smaller the strain signal, the smaller the area under the graph. Magnesium AM60 has minor increment of area under graph, which is attributable to its brittle properties in comparison with Aluminium 6061-T6, which is a ductile material. Value of strain energy is dependent on the energy absorbed [44], whereas the energy absorbed depends to the material

yield strength, tensile strength, and ductility properties [45]. Value of area under PSD graph in every thickness reacted the same to the increment of impact speed, where it decreases along the way. PSD value is dependent on the strain and impact duration value particularly, where higher PSD value was due to higher strain value and impact duration [36].

4.3 Relation of Impact Strain Signal Pattern with Stress-Strain Curve

Material behaviour of a material was ascertained from stress–strain curve constructed. Yield point, necking point, and fracture point were identified through the curve. Yield point indicates the point where elastic deformation ends and plastic deformation begins. Necking point is the point when the material gives indication before fracture, and fracture point is the point that the material is totally failed. Figure 4 shows the stress-–strain curve for Aluminium 6061-T6 and Magnesium AM60, and their material behaviour is recognised as ductile and brittle, respectively.

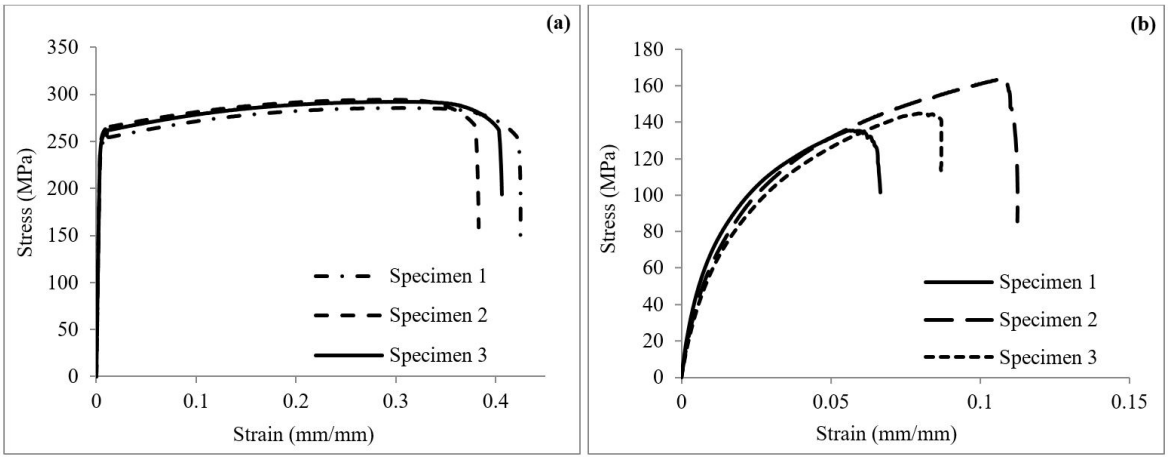

Fig. 4. Stress–strain curve for (a) Aluminium 6061-T6 and (b) Magnesium AM60

Aluminium 6061-T6 yields before strain reaches 0.008 (mm/mm) and necking point is before 0.31 (mm/mm). Unlike Aluminium 6061-T6, Magnesium AM60 has no necking point and the fracture occurs in a sudden manner, and thus, the tensile strength and fracture strength is the same for the Magnesium AM60. The mechanical properties are summarised in Table 7.

Table 7
Tensile strength and load of the material

Mechanical properties	Aluminium 6061-T6	Magnesium AM60
Ultimate tensile strength (MPa)	290.72 ± 4.59	147.95 ± 14.43
Average ultimate tensile load (kN)	13.95	6.33
Yield strength (MPa)	251.66 ± 4.71	67.83 ± 4.23
Average yield load (kN)	12.08	2.90
Fracture strength (MPa)	266.00 ± 6.79	147.95 ± 14.43
Average fracture load (kN)	12.64	6.33

Aluminium 6061-T6 has greater ultimate tensile strength compared to Magnesium AM60. With respect to this condition, the former requires more stress or load to fracture than the latter. In terms of energy absorption ability, Aluminium 6061-T6 can absorb more energy because it possesses greater elastic–plastic region and tougher, compared to Magnesium AM60. Furthermore, strain energy in tensile test is the area under the stress–strain curve, and it is defined as the energy stored

in the material under axial loading. The average energy absorbed and average strain energy from the tensile test are listed in Table 8.

Table 8
Strain energy and energy absorbed under tensile test

Material	Average energy absorbed (J)	Average strain energy (MPa)
Aluminium 6061-T6	135.76	113.11
Magnesium AM60	10.89	10.12

This section discusses the relation of impact strain signal obtained from the Charpy test with the stress–strain curve from the tensile test. This relationship was investigated to propose a new approach for predicting material behaviour by using instrumented Charpy test. Among all the results, the impact strain signal of 10 mm thickness at 5.18 m/s speed was chosen for the comparison study because 10 mm is the standard Charpy size specimen and mostly used in previous researchers' work. The relationship between impact strain signal and stress–strain curve for Aluminium 6061-T6, Magnesium AM60, and Carbon Steel 1050 is depicted in Figure 5, Figure 6 and Figure 7. Carbon Steel 1050 curves are taken from a previous study by Ali [35], and the study presented the graphs without discussing any similarities between them.

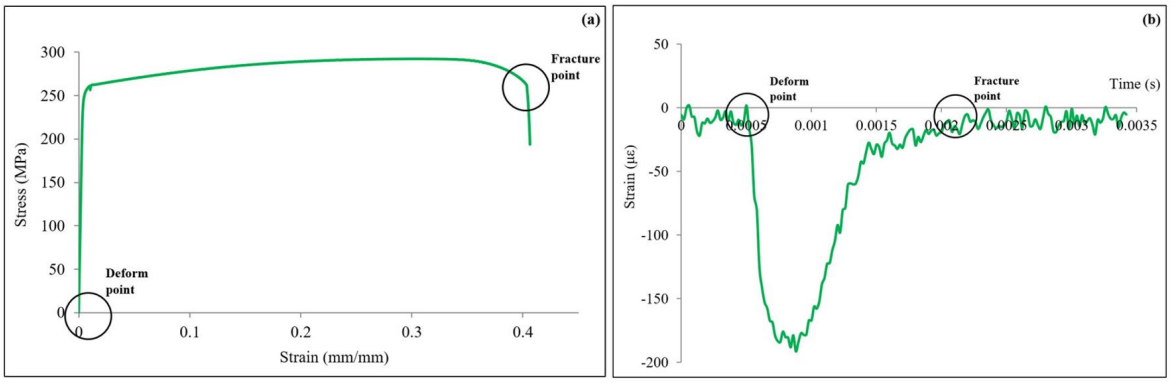

Fig. 5. Relation of impact strain signal with stress–strain curve for Aluminium 6061-T6

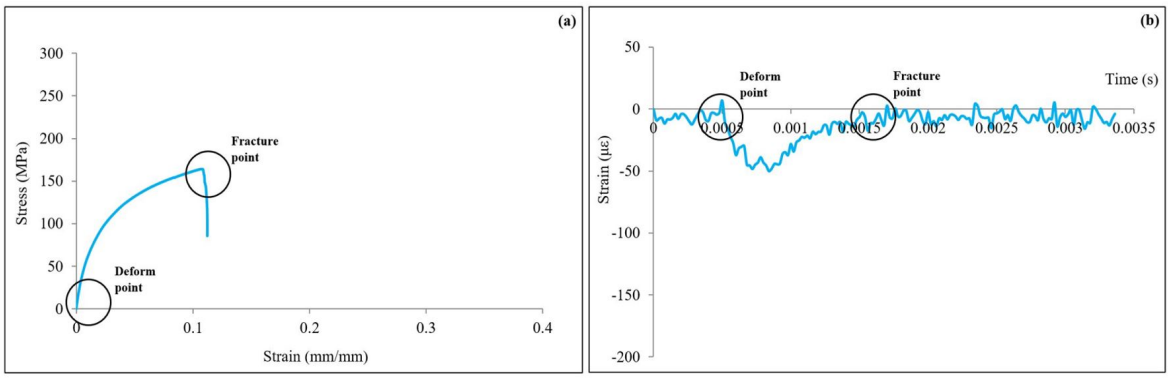

Fig. 6. Relation of impact strain signal with stress–strain curve for Magnesium AM60

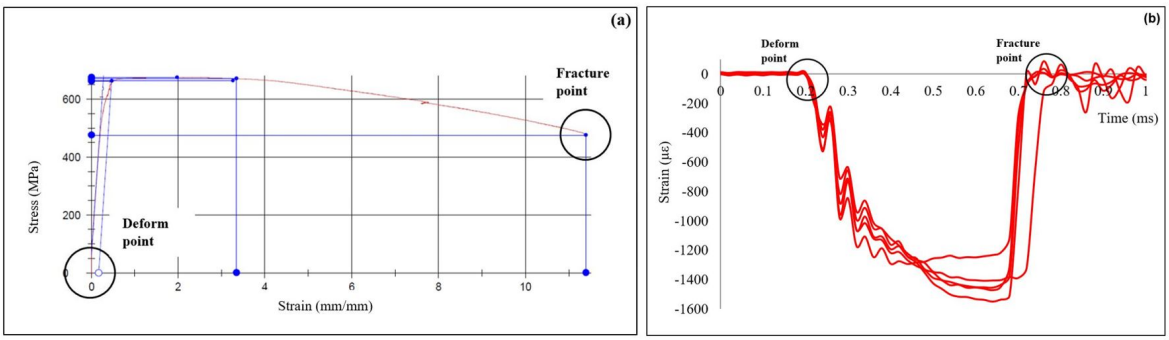

Fig. 7. Relation of impact strain signal with stress–strain curve for Carbon Steel 1050 [35]

Carbon Steel 1050 has the highest maximum strain compared to other materials as its maximum strain has a positive relationship with the Young's modulus. Young's modulus measures the stiffness of a material to predict the elongation corresponding to the material deformation or strain. Carbon Steel 1050 has Young's modulus of 210 GPa, three times higher than Aluminium 6061-T6, and 30 times higher than Magnesium AM60. These discoveries conform to the findings from Beer *et al.,* [46]. Thus, the higher the Young's modulus, the higher the maximum strain. Carbon steel is seen to have the lowest impact duration, which shows that its ductility is smaller than aluminium and magnesium.

Even though the basic mechanical process of tensile test and Charpy test are different; tension condition in tensile and compression condition in Charpy, the result for both processes failure mechanism is found to be very alike [47,48]. There is noticeable similarity between the stress–strain curve and the strain signal graph. It is the deform point and fracture point as marked in Figure 5, Figure 6 and Figure 7. Hence, the prediction on material behaviour using strain signal is achievable, together with the signal characteristics and classification.

4.4 Impact Strain Characteristics and Classification

Impact strain signal characteristics and classification is originated and referred to the parameters of the strain signal pattern in particular the energy absorbed, maximum strain, impact duration, and the area under strain–time and PSD graphs. The characterisation and classification of strain signal from Charpy test is proposed as an alternative approach to predict the material properties or behaviour, instead of the tensile test as the commonly used method. Table 9 shows the characterisation and classification of the impact strain signal at speed of 5.18 m/s with 10 mm thickness for the Aluminium 6061-T6 and Magnesium AM60, and also includes Carbon Steel 1050 from previous study by Ali *et al.,* [44].

Table 9
Characterization and classification of impact strain signal

Strain signal characteristics	Type of material		
	Aluminium 6061-T6	Magnesium AM60	Carbon Steel 1050 [35]
Energy absorbed (J)	20.40	3.60	29.60
Maximum strain (με)	−199.86	−60.02	−1435.00
Impact duration (ms)	1.74	0.86	0.55
Area under PSD graph (με2/Hz)	133.01	25.46	280.30
Area under ε–time graph (με.ms)	5840.61	383.03	–
Signal pattern/ shape	U-shaped	V-shaped	U-shaped

In general, Carbon Steel 1050 has dominated most of the characteristics with the highest value of energy absorbed, maximum strain, and strain energy, while the lowest value is shown by

Magnesium AM60. Only for impact duration, Carbon Steel 1050 has the lowest value, and the highest impact duration value is presented by Aluminium 6061-T6. In addition, the strain signal classification also shows that the materials exhibit different failure modes, identified from the Charpy test strain signal shape, which is 'U' for Aluminium 6061-T6 and Carbon Steel 1050 and 'V' for Magnesium AM60. In correlating the stress–strain curve with strain–time curve, that ductile materials, Aluminium 6061-T6 and Carbon Steel 1050 has 'U' shape of strain signal pattern, whereas brittle material, Magnesium AM60 has V-shaped strain signal pattern. With respect to this findings, further studies on the impact strain signal characteristics are necessary as to justify and establish a reliable alternative method for material behaviour prediction.

5. Conclusions

This experimental study reveals that for both materials, the energy absorption capacity is greater at low impact speed with thick specimen thickness and vice versa for thin specimen. The material thickness and impact speed applied have influenced the value of energy absorbed, impact duration, maximum strain, PSD energy, and area under the strain–time graph. As a conclusion, excluding the maximum strain, most of the results are directly proportional to the material thickness and yet inversely proportional to impact speed. As a ductile material, aluminium possess better elastic and plastic regions before the fracture occurs, and for this reason, Aluminium 6061-T6 excels in the energy absorption ability compared to Magnesium AM60. Based on the overall outcome, this study has successfully demonstrated the correlation between the energy absorbed with the area under the PSD graph and the area under the strain–time graph. The correlation provides an alternative method to solve the inaccurate and estimation of the material toughness measurement. Increase in energy absorbed caused larger amount of area under PSD graph and area under strain–time graph. The thick material impacted produces great energy absorption and larger area under graphs, though the energy absorb reduces when the loading speed goes up. This study has successfully linked the strain signal pattern from Charpy test with the stress–strain curve from the tensile test. Results discovered the specimen deformation point and fracture point from both graphs. Deformation point happens at the state where elongation and impact start, so both materials pointed at similar strain zero value. By observing the identified fracture points, both materials exhibit different strain at fracture point and time, where the aluminium experienced larger strain and longer time when compared to the magnesium. Consequently, the strain signal pattern from instrumented Charpy test can be used as another approach, a possible alternative to predict the material behaviour instead of executing the tensile test.

Acknowledgement

This work is partially supported by the Fundamental Research Grant (FRGS/1/2020/TK0/UTEM/02/36) from Malaysia's Ministry of Higher Education. The authors would like to thank Universiti Teknikal Malaysia Melaka (UTeM) for the support and to the reviewers who greatly helped produce this manuscript.

References

[1] Said, Nurlaela Muhammad, Mohd Basri Ali, and Kamarul Ariffin Zakaria. "Correlation of absorb energy with PSD energy and area under strain-time graph." *Journal of Advanced Research in Fluid Mechanics and Thermal Sciences 49,* no. 2 (2018): 126-137.

[2] Kim, Dong-Kuk, and Sunghak Lee. "Impact energy absorption of 6061 aluminum extruded tubes with different cross-sectional shapes." *Materials & design 20, no. 1* (1999): 41-49. https://doi.org/10.1016/S0261-3069(98)00042-9

[3] Alkhatib, Sami E., Faris Tarlochan, Ahmed Hashem, and Sadok Sassi. "Collapse behavior of thin-walled corrugated tapered tubes under oblique impact." *Thin-Walled Structures 122* (2018): 510-528. https://doi.org/10.1016/j.tws.2017.10.044
[4] Alqwasmi, Nouman, Faris Tarlochan, and Sami E. Alkhatib. "Study of mild steel sandwich structure energy absorption performance subjected to localized impulsive loading." *Materials 13, no. 3* (2020): 670. https://doi.org/10.3390/ma13030670
[5] Tarlochan, F., F. Samer, A. M. S. Hamouda, S. Ramesh, and Karam Khalid. "Design of thin wall structures for energy absorption applications: Enhancement of crashworthiness due to axial and oblique impact forces." *Thin-Walled Structures 71* (2013): 7-17. https://doi.org/10.1016/j.tws.2013.04.003
[6] Ferdynus, Miroslaw, Patryk Rozylo, and Michal Rogala. "Energy absorption capability of thin-walled prismatic aluminum tubes with spherical indentations." *Materials 13, no. 19* (2020): 4304. https://doi.org/10.3390/ma13194304
[7] Sofi, M. M. "A review on energy absorption of multi cell thin walled structure." *Journal of Advanced Review on Scientific Research 16* (2015): 18-24.
[8] Ghazali, N. D., and M. R. Said. "Crushing modes of aluminium tubes under axial compression using finite element analysis." *Journal of Advanced Manufacturing Technology (JAMT) 12, no. 1 (2)* (2018): 259-270.
[9] Lu, Shuo. "Impact energy absorption analysis of different thin-walled tubes with and without reinforcement." *The University of Manchester (United Kingdom),* (2014).
[10] Sun, Hongtu, Jian Wang, Guozhe Shen, and Ping Hu. "Energy absorption of aluminum alloy thin-walled tubes under axial impact." *Journal of Mechanical Science and Technology 30* (2016): 3105-3111. https://doi.org/10.1007/s12206-016-0619-2
[11] Tarlochan, F., F. Samer, A. M. S. Hamouda, S. Ramesh, and Karam Khalid. "Design of thin wall structures for energy absorption applications: Enhancement of crashworthiness due to axial and oblique impact forces." *Thin-Walled Structures 71* (2013): 7-17. https://doi.org/10.1016/j.tws.2013.04.003
[12] Muhammad Nasiruddin, S., A. Hambali, J. Rosidah, W. S. Widodo, and M. N. Ahmad. "A review of energy absorption of automotive bumper beam." *Journal of Applied Engineering Research 12* (2017): 238-245.
[13] Graciano, Carlos, Gabriela Martínez, and Edwar Saavedra. "Effect of elastoplastic behavior on the impact response of expanded metal tubes." *Dyna 83, no. 198* (2016): 102-109. https://doi.org/10.15446/dyna.v83n198.50010
[14] Borges, Helio, Gabriela Martínez, and Carlos Graciano. "Impact response of expanded metal tubes: A numerical investigation." *Thin-Walled Structures 105* (2016): 71-80. https://doi.org/10.1016/j.tws.2016.04.005
[15] Kruger, Eduardo Leira, and Ruis Camargo Tokimatsu. "Instrumented Charpy Test- Evaluation of the Force Signal Captured in the Measure Dynamic Fracture Toughness of Metallic Materials." (2003).
[16] Chang, C. L., and S. H. Yang. "Finite element simulation of wheel impact test." *Journal of Achievements in Materials and Manufacturing Engineering 28, no. 2* (2008): 167-170.
[17] Vinothkumar, S., Sabarinathan Srinivasan, and AnilKumar Nesarikar. "Simulation and test correlation of wheel impact test." *No. 2011-28-0129. SAE Technical Paper,* (2011).
[18] Ali, M. B., Kamarul Ariffin Zakaria, Shahrum Abdullah, and M. R. Alkhari. "Correlation of Impact Energy from Instrumented Charpy Impact." *Applied Mechanics and Materials 815* (2015): 221-226. https://doi.org/10.4028/www.scientific.net/AMM.815.221
[19] Murali, G., A. S. Santhi, and G. Mohan Ganesh. "Empirical relationship between the impact energy and compressive strength for fiber reinforced concrete." (2014).
[20] Tarigopula, Venkatapathi, Magnus Langseth, Odd Sture Hopperstad, and Arild Holm Clausen. "Axial crushing of thin-walled high-strength steel sections." *International Journal of Impact Engineering 32, no. 5* (2006): 847-882. https://doi.org/10.1016/j.ijimpeng.2005.07.010
[21] Nagel, G. M., and D. P. Thambiratnam. "Dynamic simulation and energy absorption of tapered tubes under impact loading." *International Journal of Crashworthiness 9, no. 4* (2004): 389-399. https://doi.org/10.1533/ijcr.2004.0298
[22] Khalid, Hasmawi, and Norhayati Ibrahim. "Charphy Impact of Medium Molecular Weight Phenol Formaldehyde (MMwPF) Plywood." *Journal of Advanced Research in Applied Sciences and Engineering Technology 18, no. 1* (2020): 24-30. https://doi.org/10.37934/araset.18.1.2430
[23] Shterenlikht, Anton, Sayyed H. Hashemi, John R. Yates, Ian C. Howard, and Robert M. Andrews. "Assessment of an instrumented Charpy impact machine." *International Journal of Fracture 132* (2005): 81-97. https://doi.org/10.1007/s10704-004-8144-1
[24] Alar, Željko, Davor Mandić, Andrija Dugorepec, and Matija Sakoman. "Application of instrumented Charpy method in characterisation of materials." *Interdisciplinary Description of Complex Systems: INDECS 13, no. 3* (2015): 479-487. https://doi.org/10.7906/indecs.13.3.12
[25] Alar, Željko, and Davor Mandić. "Comparasion of Impact and Tensile Properties of High-Strength Steel." *Metals 8, no. 7* (2018): 511. https://doi.org/10.3390/met8070511

[26] Ramli, Mohd Irman, Mohd Zaki Nuawi, Mohammad Rasidi Mohammad Rasani, Shahrum Abdullah, Muhamad Arif Fadli Ahmad, and Muhammad Fazrin Abdullah. "Development of polymer mechanical properties characteristics using I-kaz 4D analysis method." *Jurnal Teknologi 80 (3)* (2018): 29–40. https://doi.org/10.11113/jt.v80.10373
[27] Shu, Dong Wei, and Iram Raza Ahmad. "Magnesium alloys: an alternative for aluminium in structural applications." *Advanced Materials Research 168* (2011): 1631-1635. https://doi.org/10.4028/www.scientific.net/AMR.168-170.1631
[28] Mallick, P. K. "Advanced materials for automotive applications: An overview." *Advanced materials in automotive engineering* (2012): 5-27. https://doi.org/10.1533/9780857095466.5
[29] Musfirah, A. H., and A. G. Jaharah. "Magnesium and aluminum alloys in automotive industry." *Journal of Applied Sciences Research 8, no. 9* (2012): 4865-4875.
[30] Kumar, D. Sameer, and K. N. S. Suman. "Selection of magnesium alloy by MADM methods for automobile wheels." *International Journal of Engineering and Manufacturing 2* (2014): 31-41. https://doi.org/10.5815/ijem.2014.02.03
[31] Hirsch, Jürgen. "Recent development in aluminium for automotive applications." *Transactions of Nonferrous Metals Society of China 24, no. 7* (2014): 1995-2002. https://doi.org/10.1016/S1003-6326(14)63305-7
[32] Yahaya, Shamy Nazrein Md, I. I. Azmi, Chuan Huat Ng, Chee Fung Lai, Mohd Yussni Hashim, A. Adam, R. Baehr, and Karl Heinrich Grote. "An overview on forming process and heat treatments for heat treatable aluminium alloy." *Journal of Advanced Research in Fluid Mechanics and Thermal Sciences 70, no. 1* (2020): 112-124. https://doi.org/10.37934/arfmts.70.1.112124
[33] Jiang, Xin, Hai Liu, Rui Lyu, Yoshio Fukushima, Naoki Kawada, Zhenglai Zhang, and Dongying Ju. "Optimization of magnesium alloy wheel dynamic impact performance." *Advances in Materials Science and Engineering 2019* (2019). https://doi.org/10.1155/2019/2632031
[34] Abdullah, N. A. Z., M. S. M. Sani, M. S. Salwani, and N. A. Husain. "A review on crashworthiness studies of crash box structure." *Thin-Walled Structures 153* (2020): 106795. https://doi.org/10.1016/j.tws.2020.106795
[35] Ali, M. B. "Analisis Isyarat Data Terikan Impak Menggunakan Pencirian Tenaga." *Universiti Kebangsaan Malaysia. (*2013).
[36] Ali, M. B., Shahrum Abdullah, Mohd Zaki Nuawi, and A. K. Ariffin. "Correlation of absorbed impact with calculated strain energy using an instrumented Charpy impact test." (2013).
[37] Konopík, P., J. Džugan, T. Bucki, S. Rzepa, M. Rund, and R. Procházka. "Correlation between standard Charpy and sub-size Charpy test results of selected steels in upper shelf region." *In IOP Conference Series: Materials Science and Engineering, vol. 179, no. 1, p. 012039. IOP Publishing,* (2017). https://doi.org/10.1088/1757-899X/179/1/012039
[38] Yadav, Shikha, and V. K. Srivastava. "Effect of thickness and crack length on the impact behaviour of particle loaded GFRP composite." *International Research Journal of Engineering and Technology (IRJET) 2, no. 02* (2015): 115.
[39] Madhusudhan, D., Suresh Chand, S. Ganesh, and U. Saibhargavi. "Modeling and simulation of Charpy impact test of maraging steel 300 using Abaqus." *In IOP Conference Series: Materials Science and Engineering, vol. 330, no. 1, p. 012013. IOP Publishing,* (2018). https://doi.org/10.1088/1757-899X/330/1/012013
[40] Dowling, Norman E. "Mechanical Behavior of Materials eBook: International Edition." *Pearson Higher Ed,* (2013).
[41] Hirsch, Juergen, and Talal Al-Samman. "Superior light metals by texture engineering: Optimized aluminum and magnesium alloys for automotive applications." *Acta Materialia 61, no. 3* (2013): 818-843. https://doi.org/10.1016/j.actamat.2012.10.044
[42] U.S. Department of Energy. "DOE Fundamentals Handbook: Material Science." *Vol. 1. (*2016).
[43] Iváñez del Pozo, Inés, Marta María Moure Cuadrado, Shirley Kalamis García Castillo, and Sonia Sánchez Sáez. "The oblique impact response of composite sandwich plates." (2015). https://doi.org/10.1016/j.compstruct.2015.08.035
[44] Ali, M. B., S. Abdullah, Mohd Zaki Nuawi, and Ahmad Kamal Ariffin. "Investigation of energy absorbed from an instrumented charpy impact on automotive specimens." *Applied Mechanics and Materials 165* (2012): 182-186. https://doi.org/10.4028/www.scientific.net/AMM.165.182
[45] Shackelford, James F. "Introduction to materials science for engineers." *Upper Saddle River: Pearson,* (2016).
[46] Ferdinand, Beer, E. Johnston, John Dewolf, and MA David. "Mechanics of materials." *Mcgraw-Hill Education,* (2020).
[47] Tocci, Marialaura, Annalisa Pola, Lorenzo Montesano, Mattia Merlin, Gian Luca Garagnani, and G. Marina La Vecchia. "Tensile behavior and impact toughness of an AlSi3MgCr alloy." *Procedia Structural Integrity 3* (2017): 517-525. https://doi.org/10.1016/j.prostr.2017.04.053
[48] Yan, Cheng, R. X. Bai, YuanTong Gu, and W. J. Ma. "Investigation on mechanical behaviour of AM60 magnesium alloys." *Journal of Achievements in Materials and Manufacturing Engineering 31, no. 2* (2008): 398-401.